Discrete Fourier transform spreading-based generalised frequency division multiplexing

S. S. Das✉ and S. Tiwari

Generalised frequency division multiplexing (GFDM) has gained significant importance as a contender for the fifth generation (5G) air interface. The peak-to-average power ratio (PAPR) of GFDM is high due to the use of a same pulse shaping filter per subcarrier and the addition of different subcarriers at the transmitter. Proposed is the use of discrete Fourier transform (DFT) spreading-based GFDM transmission to reduce the PAPR. It is found that DFT spreading helps to reduce the PAPR of GFDM significantly. It is also seen that the bit error rate performance, which is computed through simulation and using an analytical expression of the signal-to-interference-plus noise ratio, is not compromised by DFT spreading but rather is improved in the frequency selective fading channel.

Introduction: Generalised frequency division multiplexing [1] has been shown to meet the requirements of next generation (fifth generation (5G)) mobile communication networks, such as relaxed time and frequency synchronisation, low out of band radiation, very short symbol duration and flexible bandwidth of operations [2] quite well. Therefore, it is one of the contenders for the 5G air interface.

GFDM is a block-based multicarrier transmission technology with multiple time slots. Each subcarrier is pulse shaped with a non-rectangular pulse shape to increase frequency localisation of the pulses [1]. It is shown in [3] that using the same and non-rectangular pulse shape for each subcarrier in multicarrier transmissions increases the peak-to-average power ratio (PAPR with respect to orthogonal frequency division multiplexing (OFDM). Hence, it is expected that GFDM will have a higher PAPR than OFDM for an equal number of subcarriers. The PAPR of GFDM is investigated in [4] and compared with OFDM. However, the comparison is done for an unequal number of subcarriers. The aim of this Letter is PAPR reduction for GFDM. It is shown in [5] that the discrete Fourier transform (DFT) matrix is one of the optimum precoding matrices that helps reduce PAPR in OFDM. Therefore, we investigate the effect of DFT spreading to reduce PAPR in GFDM in this Letter. Two subcarrier mapping schemes for DFT spreading [6], (i) localised frequency division multiple access (LFDMA) and (ii) interleaved frequency division multiple access (IFDMA), are considered. The bit error rate (BER) performance of DFT spreading-based GFDM system using the minimum mean square error (MMSE) receiver in frequency selective fading channels (FSFCs) is also presented. The BER of DFT spread GFDM is also obtained from an analytical expression of the signal-to-interference-plus noise ratio (SINR) developed in this Letter.

System model: A GFDM system with the total number of N subcarriers with M time slots in each block [7] is considered in this Letter. Vectors are represented by bold small letters, matrices are represented by bold capital letters and scalars are represented as normal small letters. $\boldsymbol{I}_N$ is used to represent an identity matrix of order N. Let $d_{k,m}$ be a complex valued modulated data symbol coming from the quadrature amplitude modulation (QAM) modulator having variance σ_{d}^2, where $k = 0, \ldots, N-1$ is the subcarrier index and $m = 0, \ldots, M-1$ is the time slot index. Suppose, the $MN \times 1$ vector $\boldsymbol{d} = [\boldsymbol{d}_0^{\mathrm{T}}, \ldots, \boldsymbol{d}_{M-1}^{\mathrm{T}}]^{\mathrm{T}}$ contains the data symbols of the GFDM block where the $N \times 1$ data vector $\boldsymbol{d}_i$ is constructed by concatenating N complex modulated data symbols $d_{k,i}$ of the GFDM in the frequency located at the ith time slot. The data vector $\boldsymbol{d}$ is multiplied with the precoding matrix $\boldsymbol{P}$ of size $MN \times MN$ to obtain the precoded data vector $\tilde{\boldsymbol{d}}$, i.e. $\tilde{\boldsymbol{d}} = \boldsymbol{P}\boldsymbol{d}$. Here, we consider DFT-based precoding. Therefore, $\boldsymbol{P} = \boldsymbol{P}_m\boldsymbol{P}_c$, where $\boldsymbol{P}_c$ is a block diagonal matrix with each block being a DFT spreading matrix and $\boldsymbol{P}_m$ is a permutation matrix, which is used to implement subcarrier mapping. The subcarrier mapping can be either LFDMA or IFDMA. $\boldsymbol{P}_m$ is the identity matrix for LFDMA. The precoding spreading matrix $\boldsymbol{P}_c$ can be written as

$$\boldsymbol{P}_c = \begin{bmatrix} \boldsymbol{W}_Q & 0 \ldots & 0 \\ 0 & \ddots & \vdots \\ \vdots & \ldots 0 & \boldsymbol{W}_Q \end{bmatrix}_{MN \times MN} \tag{1}$$

where $\boldsymbol{W}_Q$ is the unitary DFT matrix of size $Q \times Q$, where $Q = N/L$ is the spreading factor of the system and L is the number of DFTs used per time slot. In actual implementation, fast Fourier transform may be used instead of using the DFT matrix. The above notation only helps in formulating the system model using linear equations. The conventional GFDM system can be seen as a special case when $\boldsymbol{P} = \boldsymbol{I}_{NM}$. The symbol $g(n)$ indicates the nth sample of the MN length long pulse shaping filter. The precoded data symbol $\tilde{d}_{k,m}$ is up-sampled by N, circularly convoluted with transmitted pulse shape $g(n)$ and up-converted to subcarrier k. The transmitted samples of a data block can be given by

$$x(n) = \sum_{m=0}^{M-1} \sum_{k=0}^{N-1} \tilde{d}_{k,m} \mathrm{e}^{i(2\pi kn/N)} g((n - mN)_{MN}) \tag{2}$$

With the above, the transmitted signal for a data block can be represented in matrix form as $\boldsymbol{x} = \boldsymbol{A}\tilde{\boldsymbol{d}} = \boldsymbol{A}\boldsymbol{P}\boldsymbol{d}$, where the modulation matrix $\boldsymbol{A}$ contains all the signal processing steps involved in the modulation [7]. Let $\boldsymbol{g} = [g_0, \ldots, g_{MN-1}]^{\mathrm{T}}$ hold all the coefficients of the pulse shaping/prototype filter and g_i be the ith prototype filter coefficient. Then, $\boldsymbol{A}$ can be represented as [1], $\boldsymbol{A} = [\boldsymbol{g}_{0,0} \ \cdots \ \boldsymbol{g}_{N-1,0} \ \boldsymbol{g}_{0,1} \ \cdots \ \boldsymbol{g}_{N-1,M-1}]$ where, $g_{k,m}(n) = g(n - mN)_{MN} \mathrm{e}^{(\mathrm{j}2\pi kn/N)}$. The transmitted signal vector, $\boldsymbol{x}_{\mathrm{cp}}$, after adding the cyclic prefix (CP) of length N_{CP} to $\boldsymbol{x}$, can be expressed as $\boldsymbol{x}_{\mathrm{cp}} = [\boldsymbol{x}(MN - N_{\mathrm{cp}} + 1{:}MN)\boldsymbol{x}]$. Assuming a FSFC with impulse response length $L \le N_{\mathrm{cp}}$, the received vector of length $N_{\mathrm{CP}} + NM$ is given by $\boldsymbol{y}_{\mathrm{cp}} = \boldsymbol{h} * \boldsymbol{x}_{\mathrm{cp}} + \boldsymbol{\nu}_{\mathrm{cp}}$, where $\boldsymbol{h}$ is the channel vector, $\boldsymbol{\nu}_{\mathrm{cp}}$ is the additive white Gaussian noise (AWGN) vector of length $MN + N_{\mathrm{cp}}$ with elemental variance σ_ν^2 and '*' represents the convolution. The first N_{CP} samples of $\boldsymbol{y}_{\mathrm{cp}}$ are removed at the receiver. The signal after removal of the CP can be written as

$$\boldsymbol{y}_{MN \times 1} = \boldsymbol{H}_{MN \times MN} \boldsymbol{A}_{MN \times MN} \boldsymbol{P}_{MN \times MN} \boldsymbol{d}_{MN \times 1} + \boldsymbol{\nu}_{MN \times 1} \tag{3}$$

where $\boldsymbol{H}$ is the circulant channel convolution matrix and the subscripts indicate the dimension of the matrices.

MMSE receiver: Estimated data vector $\hat{\boldsymbol{d}}_{\mathrm{mmse}}$ for the MMSE receiver can be written as

$$\begin{aligned} \hat{\boldsymbol{d}}_{\mathrm{mmse}} &= \boldsymbol{P}^{\mathrm{H}} \underbrace{\left[\boldsymbol{I}_{MN} \frac{\sigma_\nu^2}{\sigma_d^2} + \boldsymbol{G}\right]^{-1}}_{\boldsymbol{J}} (\boldsymbol{H}\boldsymbol{A})^{\mathrm{H}} \boldsymbol{y} \\ &= \boldsymbol{P}^{\mathrm{H}} \underbrace{\left[\boldsymbol{I}_{MN} \frac{\sigma_\nu^2}{\sigma_d^2} + \boldsymbol{G}\right]^{-1}}_{\boldsymbol{B}} \boldsymbol{G}\boldsymbol{P}\boldsymbol{d} + \boldsymbol{P}^{\mathrm{H}} \underbrace{\left[\boldsymbol{I}_{MN} \frac{\sigma_\nu^2}{\sigma_d^2} + \boldsymbol{G}\right]^{-1}}_{\boldsymbol{C}} (\boldsymbol{H}\boldsymbol{A})^{\mathrm{H}} \boldsymbol{\nu} \end{aligned} \tag{4}$$

where $\boldsymbol{G} = (\boldsymbol{H}\boldsymbol{A})^{\mathrm{H}}\boldsymbol{H}\boldsymbol{A}$. The estimated lth symbol can be written as

$$\hat{d}_l = [\boldsymbol{P}^{\mathrm{H}}\boldsymbol{B}\boldsymbol{P}]_{l,l} d_l + \sum_{q=0, q \ne l}^{MN-1} [\boldsymbol{P}^{\mathrm{H}}\boldsymbol{B}\boldsymbol{P}]_{l,q} d_q + \sum_{q=0}^{MN-1} [\boldsymbol{P}^{\mathrm{H}}\boldsymbol{C}]_{l,q} \nu_t \tag{5}$$

where the first term is the desired signal, the second term is the interference and the third term is the processed noise. For the lth estimated data, for a given $\boldsymbol{H}$, the average signal power $P_{s,l} = \sigma_d^2 |[\boldsymbol{P}^{\mathrm{H}}\boldsymbol{B}\boldsymbol{P}]_{l,l}|^2$, where $|.|$ indicates the absolute value, the average interference power $P_{i,l} = \sigma_{\mathrm{d}}^2 \sum_{q=0, q \ne l}^{MN-1} |[\boldsymbol{P}^{\mathrm{H}}\boldsymbol{B}\boldsymbol{P}]_{l,q}|^2$ and the average post-processing noise power $P_{\nu,l} = \sigma_\nu^2 |[\boldsymbol{C}\boldsymbol{C}^{\mathrm{H}}]_{l,l}|^2$ (as $\boldsymbol{P}$ is the unitary matrix in our case). Since $\boldsymbol{G}$ is a Hermitian matrix, it can be diagonalised as $\boldsymbol{G} = \boldsymbol{V}\boldsymbol{\Lambda}\boldsymbol{V}^{\mathrm{H}}$, where $\boldsymbol{V}$ is a unitary matrix that holds the eigenvectors of $\boldsymbol{G}$ in its columns and $\boldsymbol{\Lambda} = \mathrm{diag}\{\lambda_0, \ldots, \lambda_i, \ldots, \lambda_{MN-1}\}$ is a diagonal matrix which holds the eigenvalues of $\boldsymbol{G}$. Therefore, the matrices $\boldsymbol{B}$ and $\boldsymbol{C}\boldsymbol{C}^{\mathrm{H}}$ can be written as

$$\boldsymbol{B} = \boldsymbol{V}' \tilde{\boldsymbol{\Lambda}} (\boldsymbol{V}')^{\mathrm{H}} \text{ and } \boldsymbol{C}\boldsymbol{C}^{\mathrm{H}} = \boldsymbol{V}' \boldsymbol{\Lambda}' \boldsymbol{V}'^{\mathrm{H}}, \text{ where } \boldsymbol{V}' = \boldsymbol{P}^{\mathrm{H}}\boldsymbol{V} \tag{6}$$

In the above

$$[\tilde{\boldsymbol{\Lambda}}]_{i,i} = \tilde{\lambda}_i = \frac{\lambda_i}{(\sigma_\nu^2/\sigma_{\mathrm{d}}^2) + \lambda_i} \text{ and } [\tilde{\boldsymbol{\Lambda}}]_{i,j} = 0, \text{ for, } i \ne j \tag{7}$$

$$[\boldsymbol{\Lambda}']_{i,i} = \lambda_i' = \frac{\lambda_i}{|\frac{\sigma_\nu^2}{\sigma_{\mathrm{d}}^2} + \lambda_i|^2} \text{ and } [\boldsymbol{\Lambda}']_{i,j} = 0, \text{ for, } i \ne j \tag{8}$$

For the AWGN channel $\boldsymbol{H} = \boldsymbol{I}$ the calculations become simpler as the eigenvalues in each matrix become identical. Hence, the trace of the matrix can be used to compute the eigenvalues. The SINR can be calculated as $\gamma = (P_{s,l}/(P_{i,l} + P_{\nu,l}))$. Using Gaussian approximation for the

processed noise and interference, the BER for M-QAM can be computed as

$$P_b(E|\gamma) \simeq 4\frac{\sqrt{M}-1}{\sqrt{M}\log_2(M)} \times \sum_{i=0}^{\sqrt{M}/2-1} Q\left((2i+1)\sqrt{\frac{3\gamma\log_2(M)}{(M-1)}}\right)$$

where γ is the SINR per bit at the receiver, Q is the Marcum Q-function, and M is the modulation order of M-QAM. The average probability of error can be found as

$$P_b(E) = \int_0^\infty P_b(E|\gamma) f_\gamma(\gamma) \mathrm{d}\gamma \tag{9}$$

where $f_\gamma(\gamma)$ is the probability distribution function of the SINR. For FSFCs, $P_b(E/\gamma)$ is computed for each symbol and averaged over several channel realisations.

Results: For performance evaluation of DFT spread GFDM, first the result of the PAPR analysis is presented which is followed by the BER performance in AWGN and then in the FSFC channel. The number of subcarriers $N = 128$ and number of time slots $M = 5$ and $Q = 4$. The roll-off factor in $g(n)$ is set as 0.5. The FSFC is considered as in [1] with a coherence bandwidth comparable with the subcarrier bandwidth. In Figs. 1–3 all curves are for GFDM-based schemes, except for the ones with the legend 'OFDM'.

The CCDF of the PAPR for different multicarrier transmission techniques is shown in Fig. 1. It first confirms that the observation of [3] is true for GFDM as hypothesised earlier, i.e. GFDM has a higher PAPR than that of OFDM for the same number of subcarriers, which is contrary to earlier reported results of the PAPR in GFDM. It is also found that the LFDMA scheme reduces the PAPR by about 2 dB, whereas the IFDMA helps to reduce the PAPR by more than 3 dB for the parameters under consideration.

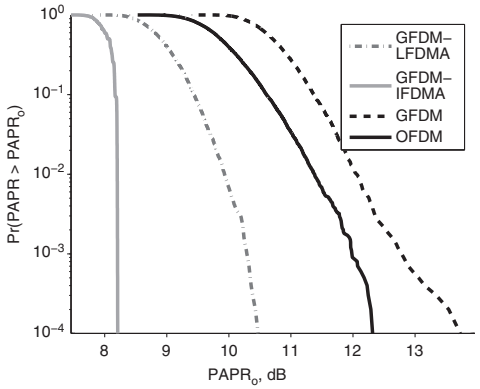

Fig. 1 *CCDF of PAPR for different multicarrier techniques*

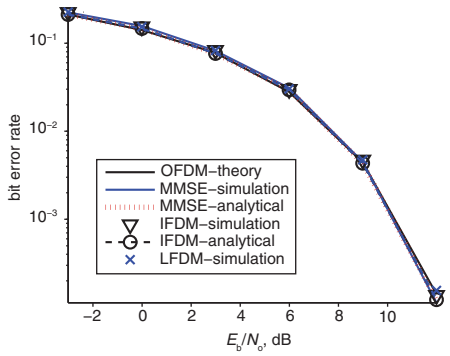

Fig. 2 *BER against E_b/N_o for 16-QAM in AWGN channel*

The BER against E_b/N_o performance of the DFT spreading-based GFDM for 16-QAM modulation using the MMSE receiver in AWGN is shown in Fig. 2. It can be observed that in the AWGN channel there is no notable difference in performance for any of the schemes considered. This is especially because the MMSE receiver is considered here. Furthermore, it is seen that the BER obtained from the analytical expression of the SINR and that of the simulation match quite well.

The BER against E_b/N_o performance in the FSFC is shown in Fig. 3. It can be observed that as in the AWGN channel, the BER obtained from the analytical expression of the SINR and that of the simulation match quite well. It also seen that the DFT spreading-based GFDM schemes have better BER performance than that of the pure GFDM-based scheme in the high E_b/N_o region. The spreading operation averages out the effect of frequency selective fading over several subcarriers. This helps the DFT spread GFDM to obtain diversity benefit in the FSFC.

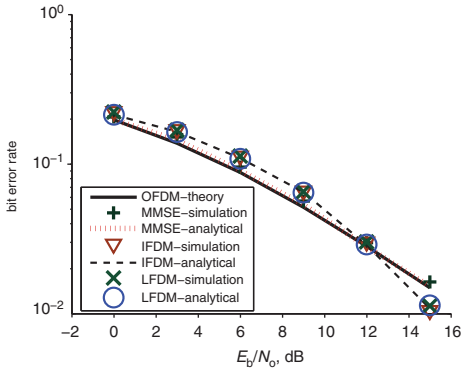

Fig. 3 *BER against E_b/N_o for 16-QAM in FSFC channel*

Conclusion: It is seen that DFT spreading helps to reduce the PAPR in GFDM significantly. The IFDMA technique of subcarrier mapping is more effective than the LFDMA in reducing the PAPR. It is also seen that DFT spread OFDM has improved BER performance in the higher SNR region in the FSFC. The BER result obtained from simulation is supported by that obtained using the analytical expression of the SNR developed in this Letter.

30 October 2014
doi: 10.1049/el.2014.3833
One or more of the Figures in this Letter are available in colour online.

S. S. Das and S. Tiwari (*Indian Institute of Technology Kharagpur, G.S. Sanyal School of Telecommunications, Kharagpur, India*)

✉ E-mail: suvra@gssst.iitkgp.ernet.in

References

1 Michailow, N., Matthe, M., Gaspar, I., Caldevilla, A., Mendes, L., Festag, A., and Fettweis, G.: 'Generalized frequency division multiplexing for 5th generation cellular networks', *IEEE Trans. Commun.*, 2014, **62**, (9), pp. 3045–3061

2 Wunder, G., Kasparick, M., Ten Brink, S., Schaich, F., Wild, T., Gaspar, I., Ohlmer, E., Krone, S., Michailow, N., Navarro, A., *et al.*: '5GNOW: challenging the LTE design paradigms of orthogonality and synchronicity'. IEEE 77th Vehicular Technology Conf., June 2013, pp. 1–5

3 Slimane, S.B.: 'Peak to average power ratio reduction of OFDM signals using pulse shaping'. IEEE Globecom, December 2000

4 Michailow, N., and Fettweis, G.: 'Low peak-to-average power ratio for next generation cellular systems with generalized frequency division multiplexing'. Int. Symp. on Intelligent Signal Processing and Communications Systems, November 2013, pp. 651–655

5 Falconer, D.: 'Linear precoding of OFDMA signals to minimize their instantaneous power variance', *IEEE Trans. Commun.*, 2011, **59**, (4), pp. 1154–1162

6 Myung, H.G., Lim, J., and Goodman, D.J.: 'Peak-to-average power ratio of single carrier FDMA signals with pulse shaping'. 17th Annual IEEE Int. Symp. on Personal, Indoor and Mobile Radio Communications, September 2006

7 Michailow, N., Krone, S., Lentmaier, M., and Fettweis, G.: 'Bit error rate performance of generalized frequency division multiplexing'. IEEE Vehicular Technology Conf. Fall, May 2012, pp. 1–5